Batteries & Supercaps

Research Article
doi.org/10.1002/batt.202400489

Chemistry Europe
European Chemical Societies Publishing

www.batteries-supercaps.org

Investigation of Electrolyte Salts in Non-Flammable Triethyl Phosphate for Sodium-Ion Batteries

Wessel W. A. Van Ekeren,[a] Lasse Dettmann,[a] Yonas Tesfamhret,[b] Andrew J. Naylor,[a] and Reza Younesi*[a]

Five different electrolyte salts, namely $NaBF_4$, $NaClO_4$, NaDFOB, NaFSI and $NaPF_6$, were evaluated in non-flammable triethyl phosphate (TEP) based electrolyte solutions in sodium-ion full-cells using high-mass loading Prussian white and hard carbon electrodes. Their impact on the viscosity, ionic conductivity and solvation structure was analyzed, revealing that NaFSI-based electrolytes exhibited a stronger interaction with TEP and less ion-pairing than the other salts, resulting in the highest ionic conductivity at a concentration of 0.8 *m* (mol/kg). Galvanostatic cycling experiments showed that none of the electrolyte salts dissolved in TEP forms an efficient passivation layer. However, adding 1 wt.% vinylene carbonate (VC) significantly improved cycling performance for the cells with $NaBF_4$, NaDFOB or NaFSI, but not with $NaClO_4$ or $NaPF_6$. Additionally, NaFSI in TEP with 1 wt.% VC electrolyte solution showed minimal gas evolution during the formation cycling (< 8 mbar). In a 1 Ah multilayer pouch cell, 0.8 *m* NaFSI in TEP with 1 wt.% VC showed promising results with 88% capacity retention after 200 cycles. X-ray photoelectron spectroscopy analysis indicated that the addition of VC results in the formation of a thin SEI and minimized TEP decomposition, particularly for 0.8 m NaFSI TEP with 1 wt.% VC. This study lays the groundwork for safer liquid electrolytes and integrating them into near-to-commercial cell setups.

1. Introduction

The interest in sodium-ion batteries is increasing rapidly worldwide, especially for large- scale stationary energy storage and low-cost transportation. Because of the practically infinite availability of sodium from the ocean, sodium-ion batteries are very promising in terms of their low-cost and environmentally friendliness.[1] However, even though sodium-ion batteries are claimed to be safer than lithium-ion batteries due to their lower energy density,[2] safety risks still exist because commercially used liquid electrolytes consist of flammable carbonate-based solvents. Recently, there has been significant research interest in the use of non-flammable liquid electrolytes as one of the strategies to address concerns in rechargeable batteries.[3] Fluorinated and alkyl phosphate-based solvents are most well-known non-flammable solvents, because of their hydrogen radical scavenging ability.[4] However, fluorinated-based solvents are not environmentally friendly and alkyl phosphate-based solvents do not form an efficient solid electrolyte interphase (SEI) during the initial electrolyte reduction at the negative electrode. To form an efficient SEI in alkyl phosphate-based electrolytes, one then needs to investigate the choice of electrolyte salt or additives.

Few of the properties that affect the salt choice are i) dissociation ability (solubility), ii) electrochemical stability vs reduction and oxidation, iii) chemical stability versus other components in the battery (electrodes, current collector), iv) safety and toxicity, and v) costs. We have previously evaluated performance of NaBOB in TEP as a promising non-flammable electrolyte.[5,6] However, here, five different salts, i.e. $NaBF_4$, $NaClO_4$, NaDFOB, NaFSI and $NaPF_6$ are studied to understand the effect of the anion on the formation and stability of the SEI in TEP based electrolyte solutions. The anion can have a significant impact on the stability of the SEI and is therefore an interesting route to investigate potentially enhanced stability of the otherwise unstable non-flammable phosphate based liquid electrolyte.[7] Ideally, the SEI is passivating the hard carbon surface, to prevent continuous decomposition of TEP, which can result in thick SEI with high resistances. The salt $NaBF_4$ is selected because of its ability to contribute to the formation of an inorganic rich SEI, which is known to be ionically conducting and electronically insulating. However, it might suffer from lower ionic conductivities due to strong interactions between Na^+ and BF_4^- In an earlier study, 1 M $NaBF_4$ in TEP with 3 wt.% VC was shown to be effective in $Na_{3.2}V_{1.8}$ $Zn_{0.2}(PO_4)_3$ (NVP) vs. hard carbon full-cell.[8] However, it has never been investigated in a high-mass loading Prussian white vs. hard carbon full-cell. $NaClO_4$ has been one of the most commonly used salts in sodium-ion batteries, because of its strong oxidation resistance, thermal stability and low costs.[9,10] Even though the commercial application might be debatable due to its toxicity and explosiveness in the dry state, this salt was selected as a fluorine free alternative. NaDFOB is one of the most promising borate salts due to its capability in forming a

[a] W. W. A. Van Ekeren, L. Dettmann, A. J. Naylor, R. Younesi
Department of Chemistry-Ångström Laboratory, Uppsala University, SE-751 21 Uppsala, Sweden
E-mail: reza.younesi@kemi.uu.se

[b] Y. Tesfamhret
Altris AB, Kungsgatan 70b, 753 18 Uppsala, Sweden

Supporting information for this article is available on the WWW under https://doi.org/10.1002/batt.202400489

Research Article
doi.org/10.1002/batt.202400489
Chemistry Europe
European Chemical Societies Publishing

passivating SEI and with better solubility than NaBOB due to the presence of electron-withdrawing fluorine, but has high costs.[11,12] Another promising and more widely studied salt is NaFSI, which has high thermal stability and has been shown to form inorganic rich SEI due to favorable FSI^- reduction, but can cause aluminum corrosion.[13,14] The most commonly used salt is $NaPF_6$ because of its good dissociation (high ionic conductivity in carbonate-based solvents), but it suffers from hydrolysis to yield PF_5, POF_3, and HF. This salt was selected for comparison reasons as most commonly used electrolyte salt for sodium-ion batteries.

Besides the investigation of various anions on improving the stability of TEP, the effect of addition of 1 wt.% vinylene carbonate (VC) is investigated, which should decompose prior to TEP and form a thin protective SEI layer.[15,16] The addition of VC to TEP based electrolytes has been studied before, but to the best of our knowledge, it has never been tested in a systematic way comparing the effect of various salts.

The aim of this study is to investigate suitable electrolyte salts by examining their fundamental physicochemical properties as well as evaluating their practical performance through electrochemical measurements and SEI analysis. These salts are studied in combination with non-flammable TEP solvent, along with the addition of 1 wt. % VC as a SEI forming additive. This work thereby provides insights into the development of safe liquid electrolytes using TEP as the main electrolyte solvent.

2. Results and Discussion

2.1. Physicochemical Properties

Ionic conductivity and viscosity are two fundamental parameters of liquid electrolytes. Figure 1a–b illustrates the effect of different electrolyte salts on these properties. For all the electrolyte salts, the highest ionic conductivity is obtained at a concentration of 0.8 m. The order of ionic conductivity observed is $NaFSI > NaDFOB > NaPF_6 > NaClO_4 > NaBF_4$, with NaFSI in TEP reaching a maximum ionic conductivity of ~6.5 mS/cm. This is a striking result, as it challenges the conventional use of 1.0 m salt concentration. Typically, a liquid electrolyte with high ionic conductivity exhibits low dynamic viscosity. However, an interesting trend is observed when comparing the ionic conductivity to the viscosity: low viscosity does not necessarily correlate with high ionic conductivity. For instance, the $NaBF_4$ based electrolyte possess the lowest viscosity, but does not yield the highest ionic conductivity. Conversely, the NaFSI based electrolyte resulted in the highest ionic conductivity but did not have the lowest viscosity. This indicates that the well-known direct relationship between ionic conductivity and viscosity does not consistently apply to liquid electrolytes. Instead, a more complex interaction between ions and solvents influence Na^+ transport in the liquid electrolyte. In other words, the ionic conductivity, including Na^+ transport, is not solely affected by the viscosity, but also by the solvation

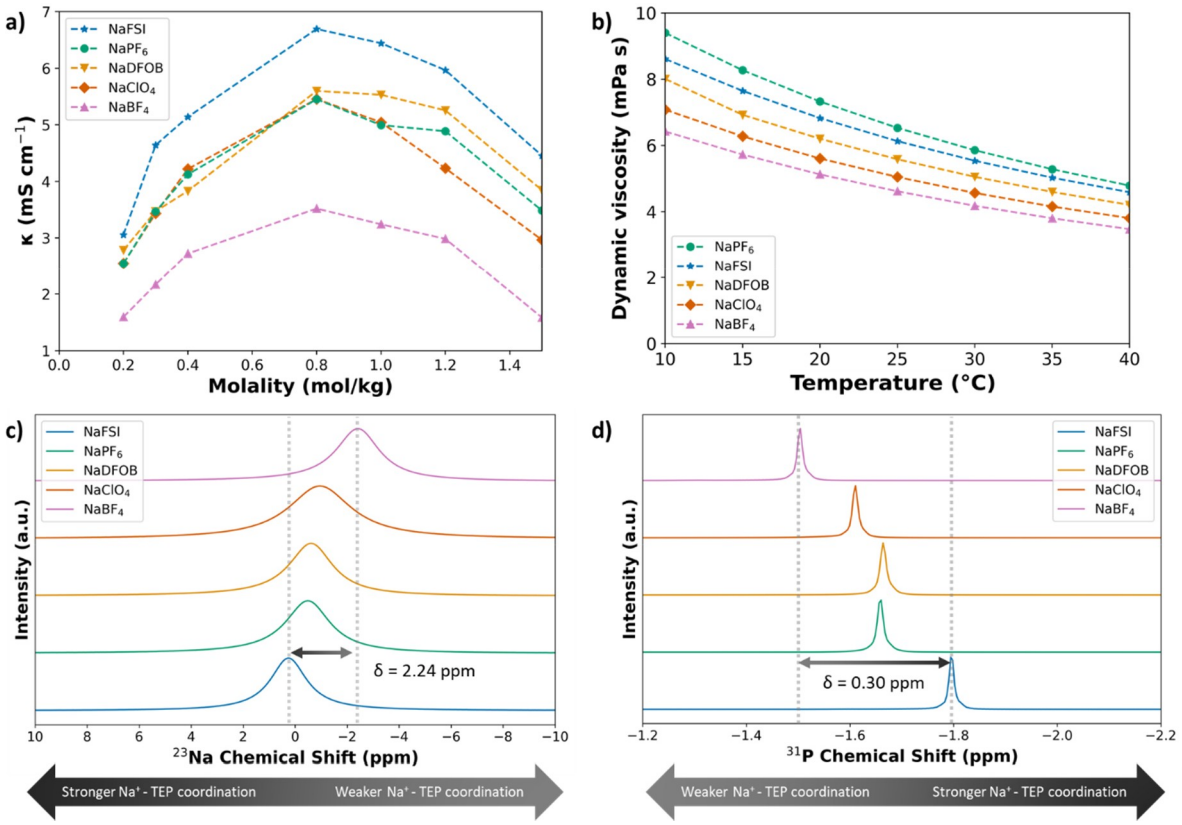

Figure 1. Physicochemical properties of the five analyzed salts in TEP. a) Ionic conductivity versus molality of five different salts measured at room temperature, b) dynamic viscosity versus temperature of 0.8 m salt in TEP, c) ^{23}Na-NMR and d) ^{31}P-NMR spectra of 0.8 m salt in TEP.

environment.[17] Specifically, the higher ionic conductivity of the NaFSI-based electrolyte can be attributed to its superior salt dissociation capability. $NaBF_4$ has a notably higher lattice energy (505 kJ mol^{-1}) compared to NaFSI (480 kJ mol^{-1}). This, combined with the solvent's ability to dissociate a certain salt, affects the formation of specific solvation structures.[18] This enhanced dissociation reduces the formation of contact-ion pairs, thereby allowing for more efficient Na^+ ion mobility within the electrolyte. To confirm this theory, ^{23}Na-NMR and ^{31}P-NMR were performed to elucidate the solvation environment around Na^+ and P═O, as shown in Figure 1c) and d), respectively. The ^{23}Na-NMR spectra reveal that Na^+ in NaFSI exhibits the strongest downfield shift due to increased Na^+-TEP interaction, whereas Na^+ in $NaBF_4$ exhibits the strongest upfield shift ($\delta = 2.24$ ppm). The ^{31}P-NMR spectra indicate that the upfield shift observed for TEP when using NaFSI results from greater d-orbital occupancy in P–O bonds when Na^+ is coordinated to TEP. This has been observed in earlier studies on Li-based electrolytes in TEP and TMP.[19,20] A more downfield shift is observed for $NaBF_4$, towards the peak of pure TEP (which appears around 0.11 ppm, as shown in a previous work by Vlad et al.), which is indicative of weaker solvation.[19] The solvation environment, therefore, plays a significant role alongside viscosity in influencing ionic conductivity. The NaFSI-based electrolyte forms a solvation structure less prone to contact-ion pair formation compared to electrolytes based on other salts like $NaBF_4$. This highlights the importance of considering both dissociation properties and solvation structures when evaluating electrolyte performance.

2.2. Galvanostatic Cycling and Cyclic Voltammetry

To evaluate the performance of different salts, galvanostatic cycling experiments were conducted in full-cells of Prussian white and hard carbon with high mass loadings (12 mg/cm^2 and 7 mg/cm^2 respectively). It was hypothesized that the various anions would contribute to the formation of different SEIs. However, none of the anions demonstrated a beneficial effect on the formation of a stable passivation layer, and the decomposition of TEP remains dominant, leading to rapid capacity fades. Consequently, further investigation was performed using the widely recognized SEI-forming additive, vinylene carbonate (VC). Figure 2 provides an overview of the galvanostatic cycling data for the five salts ($NaBF_4$, NaFSI, NaDFOB, $NaClO_4$ and $NaPF_6$), comparing the performance of each salt with and without VC additive. The highest discharge capacities were observed for the electrolyte based on $NaBF_4$, reaching close to 140 mAh/g. However, reproducibility issues were noted with this salt, indicating the need for further optimization to ensure the formation of a reproducible SEI. The NaFSI-based electrolytes showed the best reproducibility, with multiple cells reaching initial discharge capacities close to 120 mAh/g, see also Figure S1 for the long-term cycling results, reaching a capacity retention of 77% after 600 cycles. As shown in Figure 2, from the first charge-discharge curve, the overpotential is relatively high for the electrolytes based on only TEP, but this is significantly reduced with the addition of 1 wt.% VC. Notably, the efficacy of VC additive upon subsequent cycling is observed exclusively in the electrolyte based on $NaBF_4$, NaDFOB and NaFSI. Some distinct differences in voltage plateaus can be observed in the specific discharge capacity versus voltage plots in Figure S2, which indicates the formation of different SEI species for the different salts. The interplay between the anion and the SEI-forming additive emerges as the most plausible explanation for this behavior, where a certain solvation structure influences the formation of a stable SEI and a stable electrolyte structure.[21,22] The SEI was studied using X-ray photoelectron spectroscopy (XPS) to confirm these findings, which will be discussed in a later section. To further understand the selective efficacy on forming a proper passivation layer using VC additive, cyclic voltammetry was performed, providing information about the reduction potentials of the electrolyte species and the formation of a passivation layer.

The results of the first cycle of the cyclic voltammetry are presented in Figure 3. The reduction potential of TEP appears for all electrolytes around 1.2 V vs. Na^+/Na, as determined from the cyclic voltammograms without 1 wt.% VC (labelled VC-free). When 1 wt.% of VC is added, an extra reduction peak around 2.0 V vs. Na^+/Na is observed in the electrolytes based on NaFSI, NaDFOB and $NaBF_4$. This peak is absent in the electrolytes based on $NaPF_6$ and $NaClO_4$. The presence of this extra reduction peak may explain the enhanced galvanostatic cycling observed for the salts NaFSI, NaDFOB and $NaBF_4$ in TEP containing 1 wt.% VC. Also, it implies the formation of different reductive species, either as decomposition products in the liquid electrolyte or as species participating in the formation of a passivating SEI layer. The presence and interaction of different species (different anions for each salt and the presence/absence of VC) in the liquid electrolyte affect the redox potentials of the solvents. It should be noted that only 1 wt.% of VC is added to the electrolyte, meaning that VC is not always reductively decomposed before TEP.[23] Figure S3 displays cyclic voltammograms (CVs) across three cycles for a more detailed picture. It is evident that electrolytes containing NaFSI, NaDFOB, and $NaBF_4$ show a notable absence of reduction peaks in subsequent cycles, whereas $NaClO_4$ and $NaPF_6$ continue to exhibit reduction peaks. This finding confirms the formation of an effective electron-insulating layer when utilizing NaFSI, NaDFOB, or $NaBF_4$ in the non-flammable solvent mixture of TEP with 1 wt.% VC. To further investigate what species are contributing to this effective passivating layer, XPS measurements were performed.

2.3. X-Ray Photoelectron Spectroscopy

The selective enhancement observed by incorporating only 1 wt.% of VC into TEP-based electrolytes was further investigated by XPS. The SEI formed on the hard carbon surface was analyzed for the five different salts in TEP with and without 1 wt.% VC. Figure 4 represents spectra from hard carbon samples subjected to three complete formation cycles. It should be noted that the SEI is dynamic, and its composition may continue to evolve after these three formation cycles.[24,25]

Research Article
doi.org/10.1002/batt.202400489

Chemistry Europe
European Chemical Societies Publishing

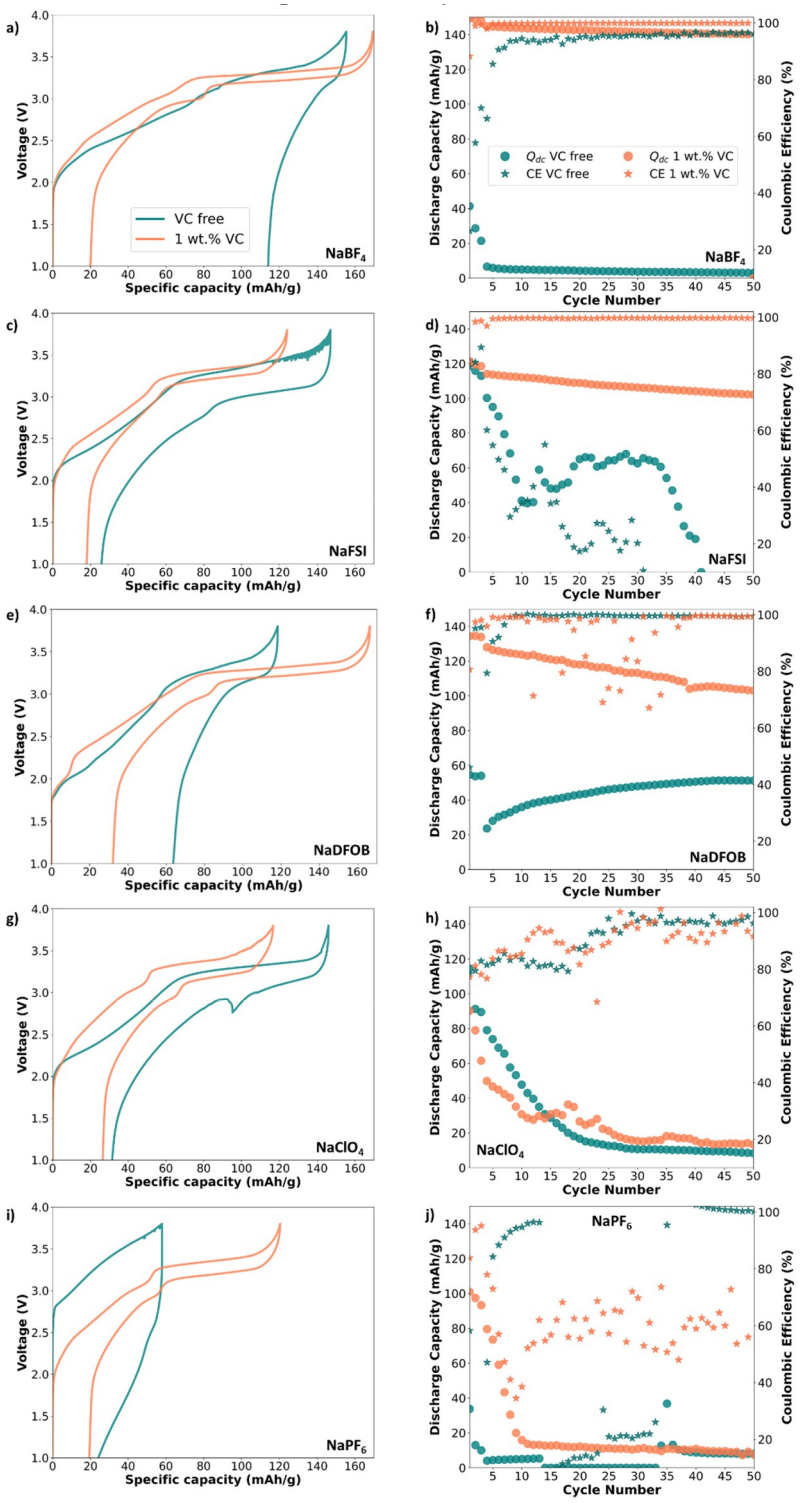

Figure 2. The galvanostatic cycling of $NaBF_4$, NaFSI, and NaDFOB in TEP electrolytes with and without 1 wt.% VC in Prussian white vs. hard carbon full-cells. In the first column the first charge/discharge curve is shown, indicating the polarization reduction using 1 wt.% VC. In the second column the discharge capacity and coulombic efficiency versus cycle are shown. a) and b) for 0.8 m $NaBF_4$, c) and d) for NaFSI, e) and f) for NaDFOB, g) and h) for $NaClO_4$, i) and j) for $NaPF_6$.

However, the XPS spectra provide a useful comparison of differences in chemistry of SEI formed using the five salts. The C 1s, F 1s, O 1s, and P 2p spectra of cycled hard carbons are shown in Figure 4, while the C 1s and survey spectra of pristine hard carbon are provided in Figure S4 and S5. The B 1s spectra can be found in the Figure S6, for more details on the boron species formed using $NaBF_4$ and NaDFOB.

The C 1s spectra reveals a shift in the peak at 284 eV, corresponding to sp2 hybridized C=C bond in the pristine sample, to 283 eV in the cycled samples. This can be explained

Research Article
doi.org/10.1002/batt.202400489
Chemistry Europe
European Chemical Societies Publishing

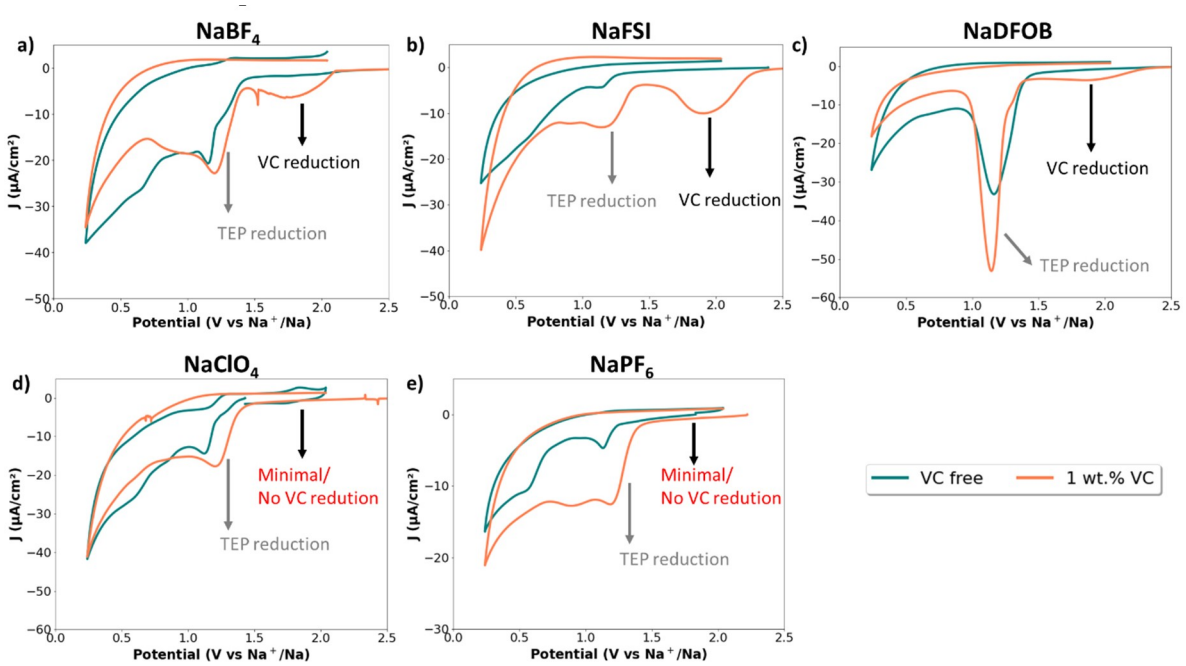

Figure 3. The cyclic voltammetry diagrams of a) $NaBF_4$, b) NaFSI, c) NaDFOB, d) $NaClO_4$ and e) $NaPF_6$ in TEP electrolytes with and without 1 wt.% VC.

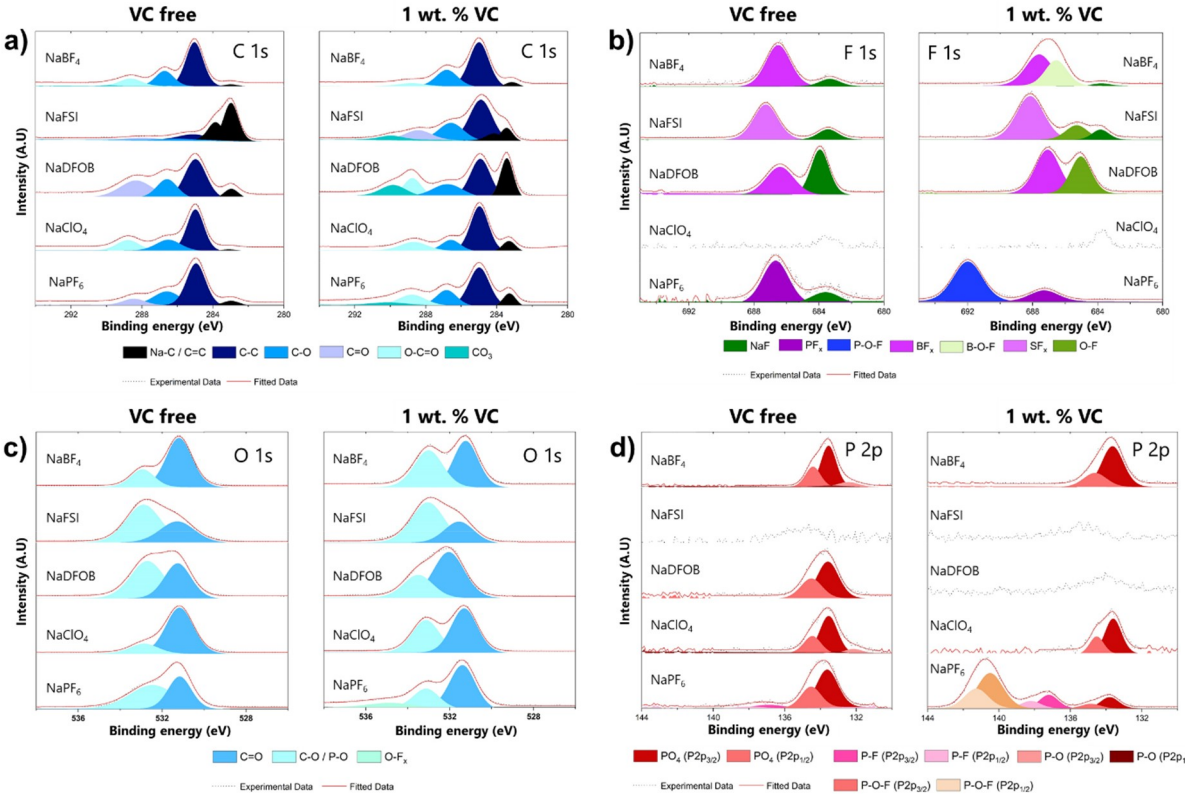

Figure 4. XPS spectra of hard carbon in the discharged state after three formation cycles measured using an excitation energy of 2.35 keV. a) C 1s spectra, b) F 1s spectra, c) O 1s spectra, and d) P 2p spectra.

either by remaining Na in the structure (Na–C) or by an electric potential gradient at the interface between the SEI and the bulk material, or by a combination of both factors.[26,27] When comparing the C 1s spectra for VC-free and 1 wt.% VC samples, the contribution from C=C bond of hard carbon increased for all samples for VC containing electrolytes, except for the NaFSI-based electrolyte. In the case of NaFSI-based electrolytes, a thin SEI is already formed without VC additive. A low relative

intensity of the peak at 283 eV indicates a relatively thick SEI for hard carbon cycled with VC-free electrolytes (except for NaFSI). The VC-free electrolytes using $NaBF_4$ or $NaClO_4$ exhibit a low intensity peak at 283 eV, indicating an SEI thickness close to or greater than 18 nm, based on the probing depth of hard X-rays with a photon energy of 2.35 keV.[28] A high ionic resistance is often associated with a thick SEI, potentially explaining the poor cycling performance observed for the VC-free electrolytes.[29] From the formation cycling in Figure S7, it can be observed that NaFSI in VC-free based electrolyte outperformed the other electrolyte solutions, which can be attributed to the more thin and protective SEI. The thinnest SEI is obtained using NaFSI, followed by NaDFOB, $NaPF_6$, $NaBF_4$ and $NaClO_4$. To ensure a less resistive and more protective SEI formed, the composition of SEI must be considered, since for instance carbonate species are known to be more passivating than other species.[30,31] First, it can be concluded that the main species formed via the electrolyte reduction in the VC containing electrolytes are similar for all the salts, except for NaFSI, which lacks the ester peak (O–C=O, ≈289 eV) and instead shows a small carbonyl peak (C=O, ≈287 eV).[32,33] Additionally, $NaBF_4$ and $NaClO_4$ show no inorganic carbonate peaks (CO_3, ≈290 eV). For NaFSI, the C=O and CO_3 peaks are only detected when VC is added to the sample, and the peak remains absent in the VC-free sample. Furthermore, increased amounts of O–C=O and inorganic carbonate (CO_3, ≈290 eV) are present in the SEI for NaFSI, NaDFOB and $NaPF_6$ based electrolytes, which is attributed to the reduction of VC.[16]

The typical SEI components can also be observed in O 1s spectra: C=O, C–O, P–O, and O–F_x.[34] The detected peaks in the O 1s were consistent with the peaks found in the C 1s spectra. For instance, the C=O in O 1s was also present in the C 1s spectra as C=O or O–C=O. Across all salts, the O 1s spectra show similar peak positions, indicating the presence of similar oxygen species. However, in the case of NaFSI, the ether-oxygen (≈533 eV) shows higher intensity than the carbonyl-oxygen (≈531 eV), which is the opposite of the trend observed with the other salts. In the electrolyte based on NaDFOB, a notable change in peak shape is seen, where the shoulder contributing to C=O increases in intensity for the VC containing electrolyte. This change correlates with the peaks in the C 1s, where for NaDFOB salt an increase in O–C=O (289 eV) and CO_3 (290 eV) was detected. It should also be noticed that, although small, a component at ≈535 eV is present for the $NaPF_6$ sample with 1 wt.% VC, which is assigned to fluorinated oxygen species (O–F_x).

From the F 1s spectra, the most significant effect is observed in the $NaPF_6$-based electrolytes, where the addition of 1 wt.% VC results in the appearance of a peak at 692 eV (P–O–F). This is presumably attributed to the reaction between VC and PF_6^-. Another distinct feature is seen for NaFSI, where an O–F peak appears around 684.5 eV after addition of 1 wt.% VC. Interestingly, in the NaDFOB VC-free sample the NaF peak is significantly larger than for the other salts. The small NaF peak in the spectra for $NaClO_4$ is attributed to trace fluorine impurities in the electrolyte, leading to NaF formation. Furthermore, the inorganic fluorine species formed differ based on the anion. For $NaBF_4$, the inorganic species are mainly found around 687 eV, which are attributed to BF_x.[35] For NaFSI, the peak appears at slightly higher binding energies, corresponding to SF_x species.[32] These differences in inorganic fluorine species highlight the differences in cleavage upon the application of an electrochemical potential, where it appears that the B–F bond in NaDFOB is most prone to cleavage, followed by S–F in NaFSI, P–F in $NaPF_6$ and then B–F in $NaBF_4$.[32]

The P 2p spectra of the cycled hard carbon electrodes provide important insights in the decomposition products of the TEP. The characteristic peaks at ≈134 eV is attributed to the phosphate species (PO_4) originating from TEP.[36] It is worth mentioning that while TEP can be decomposed into species which are soluble in the liquid electrolyte, the low intensity of the PO_4 peak suggests that continuous TEP reduction is effectively minimized. Among the five analyzed salts, NaFSI exhibits the lowest PO_4 peak intensity, which, along with its stable cycling performance, indicates that further reduction of TEP is minimized in both VC-free and 1 wt.% VC containing electrolytes. Increasing the salt concentration could potentially even further improve the cycling performance without need for VC. The result for the NaDFOB based electrolyte is particularly noteworthy, where in the VC-free electrolyte, a significant peak is present for PO_4 (≈134 eV), which is almost completely diminished with addition of 1 wt.% VC. This underscores the critical role of VC additive in preventing continuous decomposition of TEP. For the $NaPF_6$ salt, an additional feature apears at 138 eV, which is assigned to the PF_6^- anion decomposition.[37] Another peak at around 140 eV is attributed to P–O–F likely formed due to a reaction between PF_6 and VC, which is linked to the peak found at 692 eV in the F 1s spectra. It is notable that the formation of P–O–F species is only detected in the VC containing sample, further emphasizing the importance of interplay between the electrolyte components.

The composition of the SEI varies significantly depending on the type of salt used and the addition of 1 wt.% VC, demonstrating that the SEI formation and its composition are highly sensitive to the specific electrolyte composition. A likely explanation for this observation is the interaction between the anion of the salt and the VC additive. This interplay probably influences the SEI structure and composition, which in turn contributes to the effectiveness of the SEI in preventing further decomposition of TEP. The addition of 1 wt.% VC has a pronounced impact on the SEI formation and electrochemical performance, as revealed by XPS results. For $NaBF_4$, the presence of VC leads to some improvement, likely due to an increase in BF_x species, resulting in a more inorganic rich SEI. Both $NaClO_4$ and $NaPF_6$ show initial good performance with VC, forming SEIs rich in inorganic phosphates and fluorinated species like PO_4 and O–Fx, which contribute to early cycling stability. However, the significant capacity fade observed with these salts underscore the dynamic stability of the SEI in NIBs. NaDFOB demonstrates notable benefits from VC addition, with XPS indicating a reduction in PO_4 intensity and the formation of protective inorganic carbonates (e.g. –CO_3), which stabilize the SEI and prevent continuous TEP decomposition, leading to relatively good electrochemical performance. As shown by the

Research Article
doi.org/10.1002/batt.202400489
Chemistry Europe
European Chemical Societies Publishing

galvanostatic cycling, NaFSI in TEP with VC exhibited the most promising electrochemical performance. This is attributed to the beneficial effect of the FSI anion and the VC additive on the SEI formation, which promote the formation of inorganic carbonates and O–F species, which are presumably highly protective and conductive. The absence of species in the P 2p spectra indicate minimized TEP decomposition, and can explain the stable cycling performance in this electrolyte. Overall, the XPS results indicate that the presence of inorganic carbonates, fluorinated species, and reduced phosphate components is crucial in preventing continuous TEP decomposition and ensuring long-term electrochemical stability, particularly in NaDFOB and NaFSI based electrolytes. Furthermore, the differences observed in the XPS spectra, highlight the complex interplay between the salt anion and the additive in influencing the composition of the SEI.

2.4. *Operando* Pressure Measurements

The cell based on NaFSI showed the highest reproducibility and also has the highest ionic conductivity, so therefore it was selected as the electrolyte to investigate further, both in terms of pressure evolution as well as application in multilayer pouch cell. The *operando* pressure measurements were performed in a pressure cell, of which a detailed description is given in the experimental section. The resulting pressure evolution during formation cycling in the cells based on 0.8 *m* NaFSI TEP electrolyte with and without 1 wt.% VC is depicted in Figure 5. Remarkably, the cell containing 1 wt.% VC shows higher amounts of gaseous product compared to the VC-free cell (~7.5 mbar and 2 mbar). This could be attributed to the well-known formation of CO_2, C_2H_4, and CH_4 during VC decomposition.[38–40] Notably, in both electrolyte formulations, the pressure exhibited stabilization following formation cycling, as illustrated in Figure S8. Analysis of these measurements reveals that the primary surge in pressure, albeit modest for both electrolytes, occurs during formation cycling. Notably, the amount of gas released is relatively low in this case, which is comparable to an earlier study about the effects of additives in NaBOB TEP-based electrolytes for high-mass loading Prussian white versus hard carbon.[36] So, the use of the non-flammable TEP as a main electrolyte solvent has limited amount of gas evolution, and keeps at a low level with the addition of VC, even though the reduction of VC causes slightly higher amounts of gas evolution.

2.5. Application in Commercial Multilayer Pouch Cell

The electrolyte solution of NaFSI TEP with 1 wt.% VC was further evaluated in a multi-layer pouch cell to understand how this non-flammable liquid electrolyte performs in a commercial configuration, see a summary of the electrochemical results in Figure 6. The initial Coulombic efficiency (ICE) of the cell was about 86% and the average of subsequent Coulombic efficiencies was 99.52% with a variation of the Coulombic efficiency of each cycle varied between 99.2%–100%, see Figure 6 a. An ICE of 86% suggests that a substantial amount of sodium is lost during the first charge due to the formation of the SEI layer. It is also known that the ICE on hard carbon surfaces is typically lower than on graphite surfaces, due to hard carbon's more disordered and porous structure. This early result is promising and can be further improved via optimization of the SEI formation protocol and electrolyte additives.[41] The discharge capacity retention was 88% after 200 cycles. From Figure 6 b) it can be seen by comparing the charge and discharge curves that quite some polarization is observed in the first cycle, which stabilizes after the formation cycling. The average voltage during charge and discharge is shown in Figure 6c) and indicates minimal change up to 45 cycles, after which a more profound increase in the difference between charge and discharge voltage is observed, indicating an increase in the resistance of the cell. This increase in resistance explains the observed capacity fade. In Figure 6d) the normalized discharge capacity is shown versus cycle number. The normalized discharge capacity of 0.88 after 150 cycles indicates that the battery retains a substantial portion of its original capacity, but has experienced some degradation. The stable cycling performance and promising discharge capacities shows that a non-flammable liquid electrolyte based on TEP with 1 wt.% VC can compete with current flammable organic based liquid electrolyte in high-mass loading Prussian white vs hard carbon full-cells. It should be noted that a tradeoff between

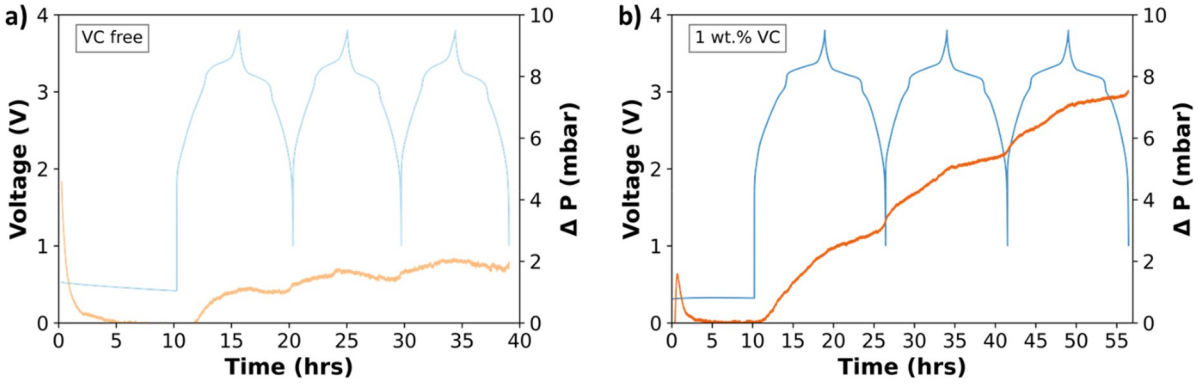

Figure 5. Pressure evolution in Prussian white vs hard carbon full cells using NaFSI TEP a) without VC and b) with VC.

Research Article
doi.org/10.1002/batt.202400489
Chemistry Europe
European Chemical Societies Publishing

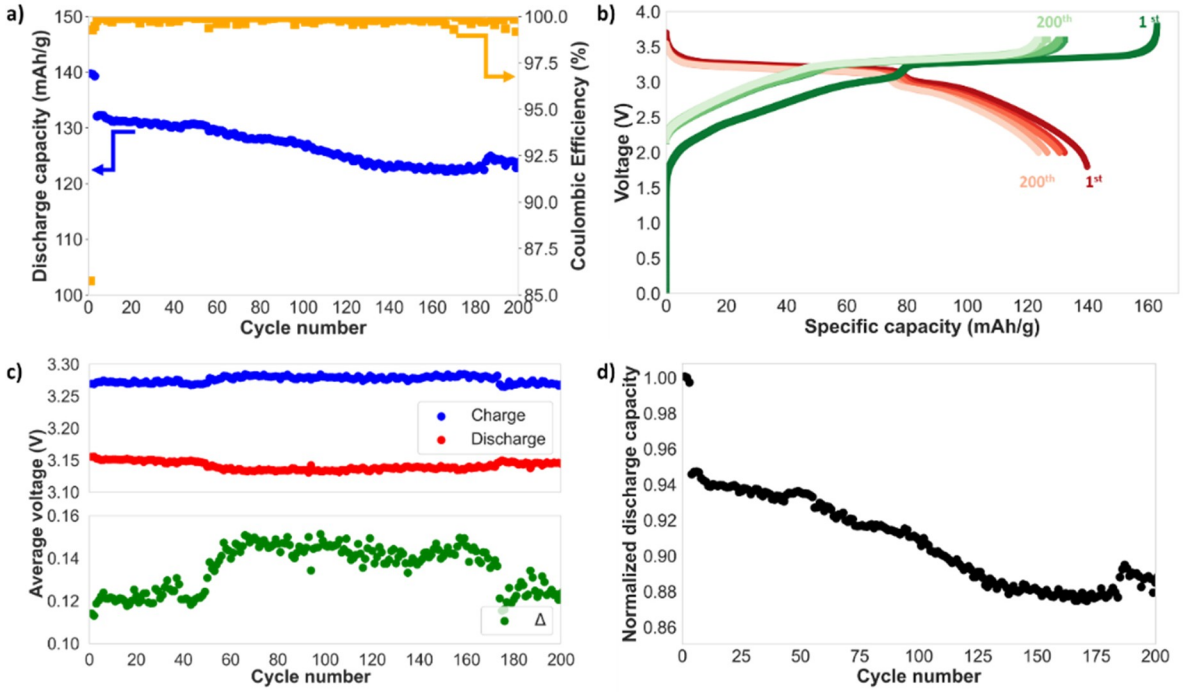

Figure 6. a) Discharge capacity and Coulombic efficiency versus cycle number b) Voltage profile versus charge and discharge capacity, c) average voltage during charge, discharge and the delta between charge and discharge, and d) the normalized discharge capacity versus cycle number.

safety and electrochemical performance most often remains, but with this type of electrolyte the gap can be minimized.

3. Conclusions

In summary, a comprehensive study was conducted to investigate the effect of five different electrolyte salts (i.e. $NaBF_4$, $NaClO_4$, NaDFOB, NaFSI and $NaPF_6$) dissolved in TEP solvent on 1) physicochemical properties and 2) minimizing the continuous TEP decomposition on hard carbon anodes. The results showed that a concentration of 0.8 m salt results in the highest ionic conductivity for all salts, challenging the conventional use of 1.0 m. The addition of 1 wt.% VC to all the electrolyte solutions was evaluated to develop a non-flammable liquid electrolyte based on TEP. Notably, the NaFSI-based electrolyte exhibited the highest ionic conductivity, attributed to a pronounced Na^+ downfield shift in the ^{23}Na-NMR spectrum. This shift suggests stronger Na^+-TEP interactions and weaker Na^+-anion interactions, promoting enhanced ion mobility. The cyclic voltammetry results revealed a reduction peak at 2.0 V vs. Na^+/Na for NaFSI, NaDFOB and $NaBF_4$ based electrolytes containing VC additive, while this peak was absent for electrolytes based on $NaPF_6$ and $NaClO_4$. The interplay between cation, anion, VC and TEP in the solvation shell of liquid electrolytes affects the reduction potential. The galvanostatic cycling results indicated that the investigated anion alone is insufficient to form a stable SEI despite that they partially influence the formation and composition of SEI. Notably, using TEP as a main electrolyte solvent without additive remains problematic due to the formation of an unstable SEI. However, the addition of 1 wt.% VC significantly improved the galvanostatic cycling performance for electrolytes based on NaFSI, NaDFOB and $NaBF_4$. This improvement is attributed to the formation of a more efficient SEI and minimized TEP decomposition. XPS measurements confirmed that the addition of 1 wt.% VC resulted in a thinner SEI and minimized TEP decomposition, particularly for NaFSI and NaDFOB. Even in high-mass loading multilayer pouch cells, the cycling performance of 0.8 m NaFSI TEP 1 wt.% VC showed high reproducibility and stable cycling with minimal gas evolution, suggesting that this non-flammable liquid electrolyte is a promising candidate for commercialization. NaFSI-based electrolytes not only resulted in more stable cycling compared to other salts, but also exhibited the highest ionic conductivity, making it particularly promising for applications where higher charge rates are desirable. Further research is required to optimize the VC concentration in this electrolyte and to comprehensively investigate the safety aspects of this non-flammable electrolyte in cell prototypes. This could include employing various methods, such as accelerating rate calorimetry (ARC), to thoroughly assess the safety implications of non-flammable electrolytes in commercial cells. This study opens new avenues for 1) further optimization of TEP based electrolytes (e.g. varying VC concentration, exploring other additives, or increasing salt concentrations) 2) conducting electrochemical tests with different electrode materials, and 3) understanding the complex interplay between anion, solvent and additive in relation to SEI formation in alkyl phosphate-based electrolytes.

Research Article
doi.org/10.1002/batt.202400489
Chemistry Europe
European Chemical Societies Publishing

Material and Methods

Preparation of Electrolytes

All salts were dried in a vacuum oven at 120 °C for 12 hours. Prior to use, the electrolyte solvent triethylphosphate (TEP, Acros, 99.8 %) was dried over dehydrated molecular sieves (4.0 Å) for at least 48 hours. All electrolyte mixing was done in an argon-filled glovebox ($O_2 < 1$ ppm and $H_2O < 1$ ppm). The electrolyte mixtures were stirred for 24 hours or until clear solutions were obtained. An overview of the chemical structures that are studied here are shown in Figure 7.

Physicochemical Properties

The viscosity and density of the electrolytes were analyzed using a Lovis 2000 M/ME (Anton Paar) operating between 10 °C and 50 °C. The conductivity measurements were carried out in the glovebox at ~25 °C using a Mettler Toledo SevenGo Duo pro pH/ORP/Ion/Conductivity meter SG78 with an InLab 738ISM probe.

Electrochemical Measurements

The electrolytes were tested in full-cell pouch configurations. Prussian white (PW, 150 mAh/g theoretical capacity) and hard carbon (HC) were dried for 15 hours under vacuum at 150 °C and 170 °C, respectively. Pouch cells were assembled using 20 mm PW, 21 mm HC electrodes, 2.5×2.5 cm Dreamweaver separator and 100 μL electrolyte in an argon-filled glovebox ($O_2 < 1$ ppm and $H_2O < 1$ ppm). The galvanostatic cycling tests were performed on a Neware BTS-4008-5 V20 mA battery tester, at room temperature (around 20 °C). The cells were kept at OCV for 10 hours prior to cycling to ensure proper wetting of the electrodes. All cells were cycled according to three formation cycles at C/10 and subsequently cycled at C/3 in the voltage range of 1.0 V–3.8 V, unless stated otherwise. A 1 Ah A7 multilayer pouch cell consisted of 14 anode layers with a dimension of 4.5×5.8 cm and 13 cathode layers with a dimension of 4.4×5.7 cm and was assembled with 8 mL of electrolyte. The formation cycling on the multilayer pouch cell were three formation cycles at C/10 in the voltage range of 1.8–3.8 V and subsequently cycled using CCCV at C/3 in the voltage range of 2.0–3.6 V, where the potential was held at 3.6 V until the current decreased in value equal to C/10.

The cyclic voltammetry measurements were performed in 3 electrode pouch cells which were assembled in an argon-filled glovebox ($O_2 < 1$ ppm and $H_2O < 1$ ppm). The counter electrode was Prussian white (12 mg/cm^2), the reference was chemically desodiated Prussian white (at 3.04 V vs Na^+/Na) and the working electrode was glassy carbon. Glassy carbon was selected as working electrode to minimize intercalation effects and focus on surface reactions resulting from the reduction of electrolyte species. Prior to use all glassy carbon electrodes were cleaned with ethanol and activated by polishing with ZrO to minimize surface adsorption. The cyclic voltammetry was performed on a Biologic potentiostat in the potential range of −3.0 V−−1.0 V at a scan rate of 0.1 mV/s. The potential window of the original cyclic voltammograms are shifted with 3.04 V to match the more convenient scale of V vs. Na^+/Na.

The operando electrochemical pressure measurements were carried out using a helium-leak tested pressure cell (PAT-Cell-Press) of El-Cell®GmbH and a Biologic potentiostat. The PAT-Cell-Press consists of a lower plunger, upper plunger and insulation sleeve which were all used as delivered by El-Cell. The plungers are made of aluminum acting as current collectors. The insulation sleeve contained a pre-dried borosilicate-glass fiber separator (Whatman®, grade GF/A, 18 mm diameter, 260 μm). The cell setup was helium-leak tested and guaranteed a maximum leakage rate of 0.3 mbar h−1. The cells were assembled with 100 mL electrolyte in an argon-filled glovebox ($O_2 < 1$ ppm and $H_2O < 1$ ppm). A slight variation in initial stack pressure of the cell might be observed, because the upper lid of the cell is closed manually, but the OCV of 12 hours ensured stable pressure prior to cycling. After assembly the cells were placed in a climate chamber (KB53, Binder (KGmbH)) and cycled at 30 °C.

X-Ray Photoelectron Spectroscopy

Samples for X-ray photoelectron spectroscopy were prepared by applying three formation cycles to PW|Hard carbon full cells at a C-rate of C/10. After fully discharging them to 1.0 V, the cells were disassembled in a glovebox and the hard carbon electrodes were washed with TEP, and dried at room temperature under vacuum for 5 hours. The samples were mounted on copper plates using conductive carbon tapes, vacuum sealed and transported to the

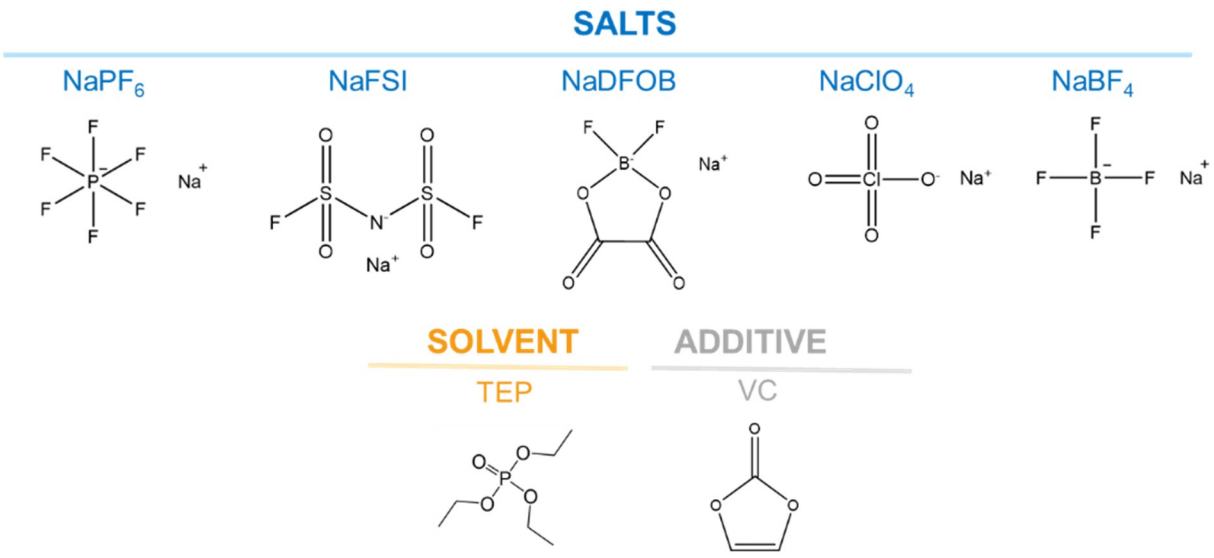

Figure 7. Overview of chemical structures of the salts, solvent and additive used in this study.

Surface and Interface Structural Analysis beamline (I09) at Diamond Light Source (Oxfordshire, UK). A transfer arm was used to move the air-sensitive samples between an argon glovebox and the beamline end-station. Photoelectron spectra were recorded for the core level transitions using a photon energy of 2.35 keV, monochromatized by a Si(111) double-crystal monochromator. The beam was spread out using defocused settings to minimize radiation damage; the spot at the sample is estimated to be approximately 300 μm (H) and up to 1 mm (W). A hemispherical VG Scienta EW4000 analyser, set to pass an energy of 200 eV, was used to record spectra. The software package CasaXPS was used for energy calibration and deconvolution of the photoelectron spectroscopy data, using a Shirley background and Gaussian-Lorentzian (GL30) fit. The C 1s spectra of the pristine sample was calibrated to the sp^2 C=C peak of hard carbon (284 eV) and the cycled samples to the sp^3 C–C peak (285 eV). The C 1s spectra for NaFSI were calibrated according to Na–C at 283 eV. All other spectra (B 1s, F 1s, O 1s and P 2p) were calibrated using the same shift observed to calibrate the C1s spectra. The P 2p peaks are split into two well-known spin orbit couples of identical species, at a distance of 0.84 eV.[39] The probing depth, three times the inelastic mean free path (IMFP) of electrons, was calculated using the TPP–M2 equation, described in detail in the NIST database.[42] The parameters of polyethylene, a low density material representative for the SEI studied here, have been used in this calculation.[43]

Author Contributions

Wessel van Ekeren: Planning, execution and data analysis of all experiments, Writing – original draft. Lasse Dettmann: Data analysis – XPS analysis. Yonas Tesfamhret: Experiments – Multilayer pouch cell. Andrew J. Naylor: Writing – review & editing, Supervision. Reza Younesi: Writing – review & editing, Supervision.

Acknowledgements

The authors would like to acknowledge the financial support by the Swedish Energy Agency via project no. 50177-1, VINNOVA via projects no. 2022-01465 and 2019-00064 (Batteries Sweden), and SuSaNa project under M-ERA-Net call 2021 (G.A. no 958174). This work was carried out with the support of Diamond Light Source, instrument I09 (proposal SI36213).

Conflict of Interests

Prussian white positive electrode material and the multilayer pouch cells used in this study were provided by ALTRIS AB, a company co-founded by R. Younesi.

Data Availability Statement

The data that support the findings of this study are available from the corresponding author upon reasonable request.

Keywords: Anion · Liquid electrolytes · Na-ion battery · Alkyl phosphate · Safety

[1] J. Y. Hwang, S. T. Myung, Y. K. Sun, *Chem. Soc. Rev.* **2017**, *46*, 3529.
[2] N. Tapia-ruiz, A. R. Armstrong, H. Alptekin, M. A. Amores, H. Au, J. Barker, R. Boston, W. R. Brant, J. M. Brittain, Y. Chen, M. Chhowalla, Y. Choi, S. I. R. Costa, M. C. Ribadeneyra, S. A. M. Dickson, E. I. Eweka, J. D. Forero-saboya, C. P. Grey, Z. Li, S. F. L. Mertens, R. Mogensen, L. Monconduit, D. M. C. Ould, R. G. Palgrave, P. Poizot, A. Ponrouch, S. Renault, E. M. Reynolds, A. Rudola, R. Sayers, D. O. Scanlon, S. Sen, V. R. Seymour, B. Silv, G. S. Stone, C. I. Thomas, M. Titirici, J. Tong, T. J. Wood, D. S. Wright, R. Younesi, *J. Phys. E* **2021**, *3*, 031503.
[3] R. Gond, W. Van Ekeren, R. Mogensen, A. J. Naylor, R. Younesi, *Mater. Horiz.* **2021**, *8*, 2913.
[4] J. W. Hastie, *J. Res. Natl. Bur. Stand. Sect. A Phys. Chem.* **1973**, *77 A*, 733.
[5] L. O. S. Colbin, R. Mogensen, A. Buckel, Y. Wang, A. J. Naylor, J. Kullgren, R. Younesi, *Adv. Mater. Interfaces* **2021**, *8*, 2101135.
[6] C. Aram Hall, L. O. S. Colbin, A. Buckel, R. Younesi, *Batteries & Supercaps* **2024**, *7*, e202300338.
[7] R. Mogensen, S. Colbin, R. Younesi, *Batteries & Supercaps* **2021**, *4*, 791.
[8] K. Du, C. Wang, P. Balaya, G. R. Satyanarayana Reddy, M. Law, *Chem. Commun.* **2022**, *58*, 533.
[9] A. Ponrouch, D. Monti, A. Boschin, B. Steen, P. Johansson, M. R. Palacín, *J. Mater. Chem. A* **2015**, *3*, 22.
[10] G. G. Eshetu, S. Grugeon, H. Kim, S. Jeong, L. Wu, G. Gachot, S. Laruelle, M. Armand, S. Passerini, *ChemSusChem* **2016**, *9*, 462.
[11] L. Gao, J. Chen, Y. Liu, Y. Yamauchi, Z. Huang, X. Kong, *J. Mater. Chem. A Mater.* **2018**, *6*, 12012.
[12] Z. Sun, W. Fu, M. Z. Liu, P. Lu, E. Zhao, A. Magasinski, M. Liu, S. Luo, J. McDaniel, G. Yushin, *J. Mater. Chem. A Mater.* **2020**, *8*, 4091.
[13] M. Goktas, C. Bolli, J. Buchheim, E. J. Berg, P. Novák, F. Bonilla, T. Rojo, S. Komaba, K. Kubota, P. Adelhelm, *ACS Appl. Mater. Interfaces* **2019**, *11*, 32844.
[14] M. Forsyth, M. Hilder, Y. Zhang, F. Chen, L. Carre, D. A. Rakov, M. Armand, D. R. Macfarlane, C. Pozo-Gonzalo, P. C. Howlett, *ACS Appl. Mater. Interfaces* **2019**, *11*, 43093.
[15] D. Aurbach, K. Gamolsky, B. Markovsky, Y. Gofer, M. Schmidt, U. Heider, *Electrochim. Acta* **2002**, *47*, 1423.
[16] L. El Ouatani, R. Dedryvère, C. Siret, P. Biensan, S. Reynaud, P. Iratçabal, D. Gonbeau, *J. Electrochem. Soc.* **2009**, *156*, A103.
[17] H. K. Bergstrom, B. D. McCloskey, *ACS Energy Lett.* **2024**, *9*, 373.
[18] Z. Tian, Y. Zou, G. Liu, Y. Wang, J. Yin, J. Ming, H. N. Alshareef, *Adv. Sci.* **2022**, *9*, 1.
[19] X. Zhang, X. Lin, P. Xu, R. Yuan, D. Gupta, R. Rupp, G. Barozzino-Consiglio, H. Xu, Q. Dong, A. Vlad, *J. Power Sources* **2022**, *541*, 231644.
[20] B. Ernould, L. Sieuw, G. Barozzino-Consiglio, J. F. Gohy, A. Vlad, *ACS Appl. Energ. Mater.* **2019**, *2*, 7879.
[21] H. Cheng, Q. Sun, L. Li, Y. Zou, Y. Wang, T. Cai, F. Zhao, G. Liu, Z. Ma, W. Wahyudi, Q. Li, J. Ming, *ACS Energy Lett.* **2022**, *7*, 490.
[22] T. Hou, G. Yang, N. N. Rajput, J. Self, S. W. Park, J. Nanda, K. A. Persson, *Nano Energy* **2019**, *64*, 103881.
[23] K. Ushirogata, K. Sodeyama, Y. Okuno, Y. Tateyama, *J. Am. Chem. Soc.* **2013**, *135*, 11967.
[24] L. A. Ma, A. Buckel, A. Hofmann, L. Nyholm, R. Younesi, *Adv. Sci.* **2024**, *11*, 2306771.
[25] L. A. Ma, A. J. Naylor, L. Nyholm, R. Younesi, *Angew. Chem. Int. Ed.* **2021**, *60*, 4855.
[26] A. Ponrouch, R. Dedryvère, D. Monti, A. E. Demet, J. M. Ateba Mba, L. Croguennec, C. Masquelier, P. Johansson, M. R. Palacín, *Energy Environ. Sci.* **2013**, *6*, 2361.
[27] J. Maibach, F. Lindgren, H. Eriksson, K. Edström, M. Hahlin, *J. Phys. Chem. Lett.* **2016**, *7*, 1775.
[28] F. Gebert, R. Lundström, W. van Ekeren, A. Naylor, *Batteries & Supercaps* **2024**, *9*, 0.
[29] P. Verma, P. Maire, P. Novák, *Electrochim. Acta* **2010**, *55*, 6332.
[30] S. J. An, J. Li, C. Daniel, D. Mohanty, S. Nagpure, D. L. Wood, *Carbon* **2016**, *105*, 52.
[31] N. Takenaka, Y. Suzuki, H. Sakai, M. Nagaoka, *J. Phys. Chem. C* **2014**, *118*, 10874.
[32] G. G. Eshetu, T. Diemant, M. Hekmatfar, S. Grugeon, R. J. Behm, S. Laruelle, M. Armand, S. Passerini, *Nano Energy* **2019**, *55*, 327.
[33] H. R. Sarma, J. Sun, I. E. Gunathilaka, Y. Hora, R. Rajkhowa, M. Forsyth, N. Byrne, *Front. Batteries Electrochem.* **2024**, *2*, 1.

[34] M. Ma, H. Cai, C. Xu, R. Huang, S. Wang, H. Pan, Y. S. Hu, *Adv. Funct. Mater.* **2021**, *31*, 2100278 .
[35] X. Yi, X. Li, J. Zhong, Z. Cui, Z. Wang, H. Guo, J. Wang, G. Yan, *ACS Appl. Mater. Interfaces* **2024**, *16*, 11585.
[36] J. Welch, R. Mogensen, W. van Ekeren, H. Eriksson, A. J. Naylor, R. Younesi, *J. Electrochem. Soc.* **2022**, *169*, 120523.
[37] K. Palanisamy, S. Daboss, J. Romer, D. Schäfer, M. Rohnke, J. K. Flowers, S. Fuchs, H. S. Stein, M. Fichtner, C. Kranz, *Batteries Supercaps* **2024**, *7*, e202300482 .
[38] L. Madec, R. Petibon, K. Tasaki, J. Xia, J. P. Sun, I. G. Hill, J. R. Dahn, *Phys. Chem. Chem. Phys.* **2015**, *17*, 27062.
[39] D. Pritzl, S. Solchenbach, M. Wetjen, H. A. Gasteiger, *J. Electrochem. Soc.* **2017**, *164*, A2625.
[40] L. Zhang, C. Tsolakidou, S. Mariyappan, J. Tarascon, *Energy Storage Mater.* **2021**, *42*, 12.
[41] A. Buckel, C. A. Hall, L. A. Ma, L. O. S. Colbin, H. Eriksson, R. Mogensen, R. Younesi, *Batter. Supercaps* **2024**, *7*, e202300533.
[42] C. K. Powell, A. Jablonski, *NIST Electron Inelastic-Mean-Free-Path Database - Version 1.2, National Institute of Standards and Technology, Gaithersburg, MD* **2010**.
[43] S. Tanuma, C. J. Powell, D. R. Penn, *Surf. Interface Anal.* **1994**, *21*, 165.

Manuscript received: July 15, 2024
Revised manuscript received: October 6, 2024
Accepted manuscript online: October 8, 2024
Version of record online: November 13, 2024